EWGAE 33rd European Conference on Acoustic Emission Testing
12-14 September 2018 - Senlis - France

32 - The sound of metal: Acoustic Emission during the deformation of commercially pure titanium

Nick Goossens[1], Marc Seefeldt[1], Martine Wevers[1]

[1] Department of Materials Engineering, KU Leuven, Kasteelpark Arenberg 44, 3001 Leuven, Belgium

Abstract:

Acoustic emission (AE) was monitored in situ during in-plane tensile deformation of a commercially pure titanium plate. Different load orientations were considered: parallel to the rolling direction (RD), transversal direction (TD) and under an angle of 45 degrees (45D) with RD. The AE event rate, peak amplitude, signal duration, rise time and ring-down counts were monitored during deformation. Orientation dependent mechanical behavior, AE signal characteristics and microstructural evolution was observed and correlated to the difference in texture and twinning phenomena. The intensity and characteristics of AE signals in RD and 45D do not change considerably during deformation, which was attributed to the continuous nucleation and growth of compression twins. Anomalous AE behavior in TD was observed, showing two distinct peaks. All signal parameters show significantly decreased values during a first peak, which was correlated to massive nucleation of small tensile twins. These tensile twins disappear with increasing strain, indicating the end of the first peak. The second peak is comparable to the plateau behavior in RD and 45D and occurs during necking. Compression twinning is dominant, but limited to the necking zone. An unfavorable textural effect in TD has been identified, which hinders the formation of compression twins during the homogeneous deformation, as opposed to RD and 45D, resulting in anomalous AE behavior. The acoustic emission technique proves to be a complementary technique to electron diffraction as it allows monitoring and identifying the twinning modes of commercially pure titanium in situ.

1. Introduction

Commercially pure titanium (CP-Ti) and titanium alloys have excellent engineering properties such as a good corrosion resistance, high specific strength and stiffness and a good biocompatibility. Therefore, titanium is extensively used in cutting-edge applications in the fields of aerospace, automotive and medicine, for instance for engine applications and medical implants. In all these applications, the material is loaded and the mechanical response has to be known precisely. For this purpose, a complete understanding on the deformation behavior of titanium is desired. However, titanium is an hexagonal metal and therefore has only access to three main slip systems: basal, prismatic and pyramidal. The von Mises criterion states that the activation of five independent slip systems is required to plastically deform polycrystals [1]. The prismatic <*a*>, pyramidal <*a*>, basal <*a*> and pyramidal <*a*+*c*> are the most common slip systems in titanium. However, <*a*> slip systems are unable to allow strain in the direction of the *c*-axis and the critical resolved shear stress of pyramidal <*a*+*c*> slip systems is high at room temperature. Therefore, twinning mechanisms have to complement dislocation slip to fulfill the von Mises criterion and allow plasticity [2,3]. The strong orientation-dependency of the activation of basal slip and particular twinning modes complicate the explanation of the entire deformation process of titanium.

Acoustic emissions (AE) are transient elastic waves that are formed by the relaxation of internal stresses, which are instantaneously imbalanced by a sudden change in the microstructure of a material [4]. AE carries information of the dynamic processes, from which they originated and which lead to plastic deformation. Twinning and the initiation of dislocation slip are known to be the principal sources of AE in titanium. AE can be measured *in situ* during the deformation of a material and therefore allows the extraction of dynamic information concerning the deformation mechanism. Because of this AE provides a dynamic complement to the classical static Electron Backscatter Diffraction (EBSD) technique, which has already been used to investigate the deformation mechanisms in magnesium alloys [5,6].

2. Description of work

A plate of hot-rolled commercially pure titanium grade 2 (0.30 wt.% Fe, 0.25 wt.% O, 0.1 wt.% C, 0.03 wt.% N, 0.015 wt.% H) having a thickness of 1 mm was used. The microstructure consists of equiaxed grains with a mean grain size of 52 µm and standard deviation of 20 µm. Two sets of three types of tensile specimens (fig. 1) were prepared with the load direction parallel to the rolling direction ("RD"), the transversal direction ("TD") and under an angle of 45° with respect to the rolling direction ("45D"). One set was used to carry out in situ AE measurements, whereas the other set was used for EBSD measurements. The tensile tests were performed on an Instron 4505 tensile machine (Instron, United States) equipped with a 100 kN load cell and a constant displacement rate of 0.5 mm min^{-1} at room temperature. The specimens were strained until failure occurred.

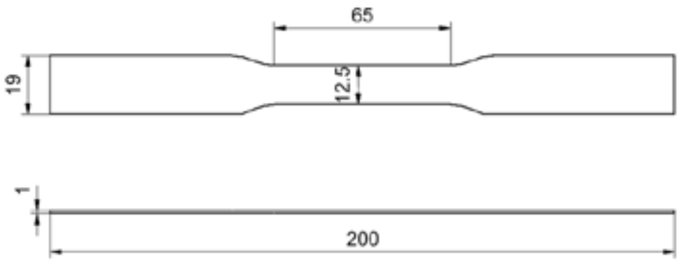

Fig. 1. Dimensions of the tensile specimens in mm.

AE was simultaneously monitored using the AMSY-5 system (Vallen Systeme, Germany). Two B1025 broadband transducers with a flat frequency response between 50 and 2000 kHz were symmetrically attached on the tensile specimens. The distance between both sensors was 100 mm. A signal threshold level of 30 dB was set just above the general noise level. Signals that were not generated in the area between both transducers, such as signals from the grips, were considered as noise and discarded by a location filter.

The microstructural evolution up to several different strain levels was investigated with automated EBSD scans using a scanning electron microscope (Nova 600 Nanolab, Thermo Fisher Scientific, United States) and TSL OIM Analyze v.8 (EDAX, United States) data acquisition and analysis software. An acceleration voltage of 20 kV and a step size of 2 µm were used. The final strain levels were chosen based on the observed AE behavior. All specimens were cut and mechanically polished after straining. In the last polishing step, a colloidal silica suspension containing 30 vol.% H_2O_2 was used. All specimens were finally polished using a VibroMet (Buehler, United States) vibratory polishing apparatus for 2 hours.

3. Results

The true stress-strain curves for the three different specimens are shown in fig. 2. Fig. 3 shows the engineering stress-strain curves together with the corresponding AE event rates (number of events per time interval). Plastic anisotropy is evidenced by a slightly larger yield stress in TD compared to RD and 45D. The elongation to failure and the rate of strain hardening (slope of the stress-strain curves) are both the largest in RD and the smallest in TD, suggesting that the plasticity is the highest in RD and the lowest in TD. Anisotropic stress-strain behavior is well-known for commercially pure titanium and attributed to the texture, resulting in the activation of different twinning systems [7-10]. Different fracture types were finally observed: the TD specimen failed by a cup-cone type fracture, while the RD and 45D specimens failed by a shear-type fracture.

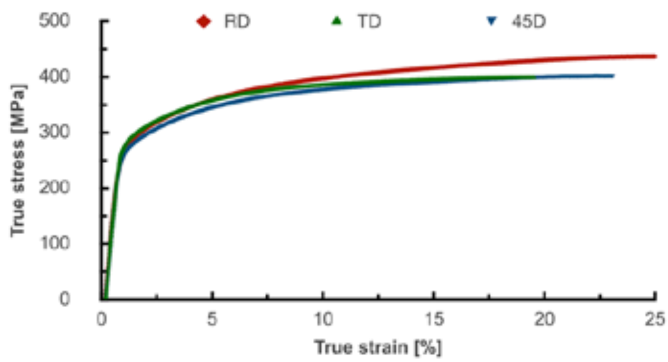

Fig. 2. True stress-strain curves of commercially pure titanium at room temperature parallel to the rolling direction (RD), transversal direction (TD) and under an angle of 45° with the rolling direction (45D).

The AE event rate curves are determined by burst-type emission, which is likely due to fast and discontinuous deformation phenomena such as twinning. An example of a typical AE burst signal is given in fig. 4. The AE response in TD differs from the RD and 45D and can be called anisotropic as well, corresponding to the mechanical behavior. The amount of detected acoustic events increases sharply at the onset of plastic deformation. In TD (fig. 3b) two maxima can now be distinguished: a first maximum around 9% strain when the ultimate tensile strength (UTS) is reached and a maximum peak around 26% strain, which coincides with the macroscopic necking of the tensile specimen. The AE response in RD (fig. 3a) and 45D (fig. 3c) is much less strain-dependent. The AE event rate increases fast to reach a plateau value, which remains nearly constant until the specimen fractures. The start of this plateau occurs when the UTS of the material is reached. Besides the shape of the curves, the magnitude of the AE event rate is remarkably different as well. It is the largest in RD, which corresponds to the outspoken strain hardening behavior. A plateau value of 81 ± 9 s^{-1} is obtained. In contrast, the lower strain hardening in TD is visible by a reduced AE event rate. At the first maximum, an event rate of 34 ± 6 s^{-1} is obtained, which is increased to 68 ± 8 s^{-1} at the second maximum. In 45D an in-between event rate of 60 ± 7 s-1 is obtained at the plateau.

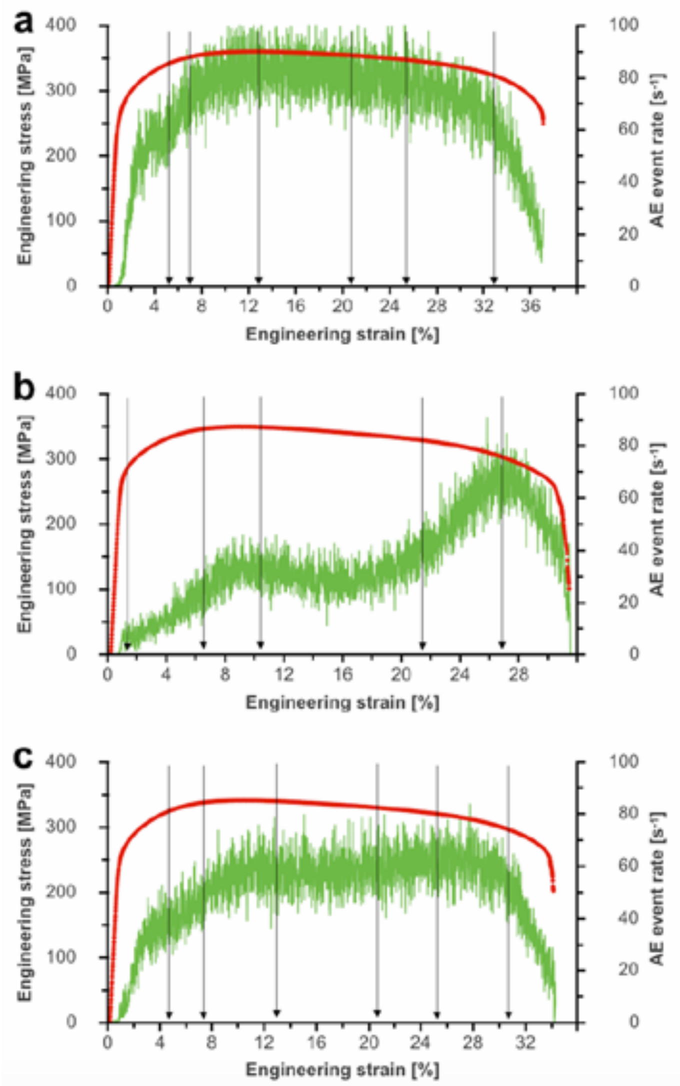

Fig. 3. Engineering stress-strain curves and corresponding acoustic emission event rate of commercially pure titanium at room temperature in a direction parallel to (a) RD (b) TD and (c) 45D. The arrows denote the strain levels at which the microstructure is investigated with EBSD.

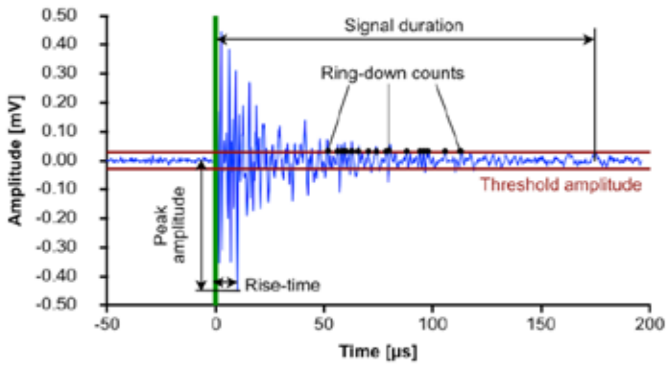

Fig. 4. Typical AE burst signal. Peak amplitude, signal duration, signal rise-time and ring-down counts are indicated. The threshold amplitude corresponds to 30 dB.

Whether the different AE response in TD translates into a different active deformation mechanism needs further investigation. Indeed, a different deformation mechanism would cause sound waves with different properties and characteristics. Therefore, the evolution of four signal parameters was monitored as a function of the strain (fig. 5) for the three different specimen orientations. Peak amplitude, signal duration, signal rise-time and the ring-down counts were considered.

A physical interpretation of these parameters is shown in fig. 4. The evolution of these parameters as a function of strain has a similar anisotropy. No outspoken change in the AE parameters occurs in RD and 45D with increased strain. Only the ring-down count has a tendency to decrease during the stage of inhomogeneous plastic deformation. Moreover, the distribution of the different signal parameters is quantitatively similar in RD and 45D. The values of the 50th and 80th percentile of the peak amplitude, signal duration, signal rise-time and the ring-down count distributions are given in table 1 for RD, 45D and TD.

	RD		45D		TD	
Percentile	50th	90th	50th	90th	50th	90th
Peak amplitude (dB)	40.0	48.7	40.0	48.5	39.9	48.4
Signal duration (μs)	53	267	50	223	43	207
Signal rise-time (μs)	5.0	13.6	5.4	11.3	7.0	13.4
Ring-down counts	12	36	11	33	10	27

Table 1. 50th and 90th percentile values of the distribution of the peak amplitude, signal duration, signal rise-time and ring-down counts of the acoustic emission measured with the load direction parallel to the rolling direction (RD), under an angle of 45° with the rolling direction (45D) and parallel to the transversal direction (TD)

The numbers for RD and 45D show that although the maximal values of all parameters in fig. 5a and fig. 5c seem to differ and appear to show large scatter, the vast majority of all the signals considered have considerably lower parameter values, which are comparable in both RD and 45D. The scatter in the values of these parameters is caused by a very small percentage of signals, which could be used to distinguish the two orientations: a larger part of the AE in RD can reach larger parameter values than the respective AE in 45D can.

The shapes of the parameter distributions obtained from AE during straining in TD are again different and show two maxima. The time (or strain) at which these maxima occur, is similar to the time (or strain) at which the maxima in the AE event rate curve (fig. 3b) occur. The maxima in the parameter distributions are less pronounced though. A similar quantitative approach is followed to compare the distributions of the AE signal parameters in TD with the earlier described distributions in the other directions (table 1). Except for the signal rise-time, all the values are lower than the respective values in the other directions. Again, the scatter in the parameter distribution is predominantly caused by a minority of the signals. To summarize, the majority of AE signals in TD have the lowest value of peak amplitude, ring-down counts and signal duration and the highest value of signal rise-time compared to the signals in RD and 45D. The same holds for the ring-down counts and signal rise-time of the minority signals. However, the highest percentile of these minority signals can achieve the largest values for the peak amplitude and the smallest values for signal rise-time. This anomaly in the parameter distribution can be better illustrated using crossplots (fig. 6), in which two independent signal parameters are plotted against each other. In this case, the ring-down counts and peak amplitude of the signals are plotted against each other.

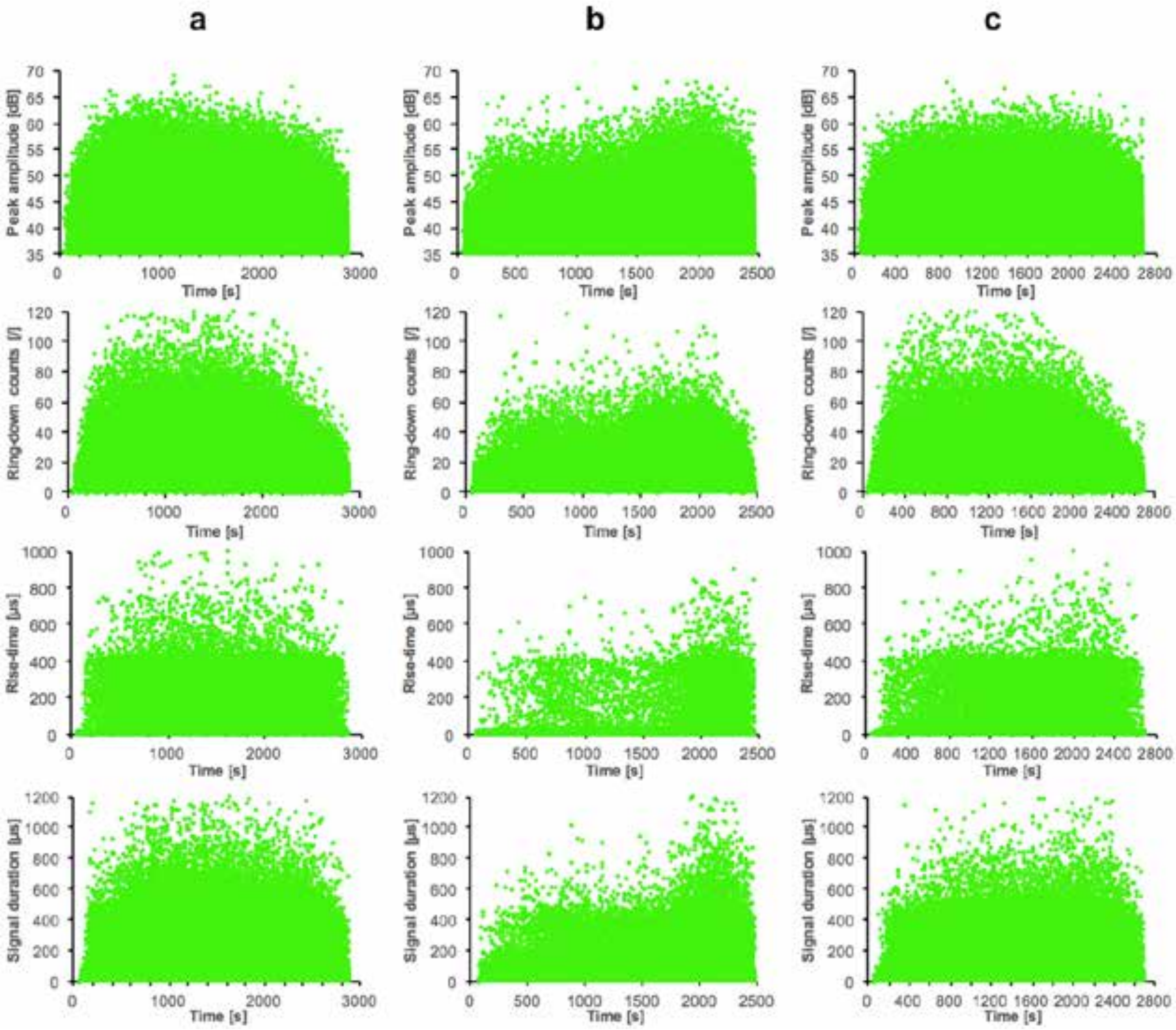

Fig. 5. Distributions of the peak amplitude, ring-down counts, signal rise-time and signal duration of the AE signals in function of time. The AE signals are received upon tensile deformation of commercially pure titanium at room temperature in a direction parallel to (a) RD (b) TD and (c) 45D.

The color code is related to the three 'deformation stages' that determine the mechanical behavior of the tensile specimens and were seen to influence the AE behavior in an anisotropic way. The blue data points correspond to the onset of plastic deformation. The green data points correspond to the moment when the UTS of the material is reached. Finally, the red datapoints correspond to the period during which macroscopic necking is observed. While the green and red region almost completely overlap for RD (fig. 6a) and 45D (fig. 6c) specimens, the red region is clearly stretched out more towards larger peak amplitudes than the green region for TD (fig. 6b) specimens. This essentially confirms the time (thus strain) indifference of the parameters in RD and 45D and the large similarities between those two orientations.

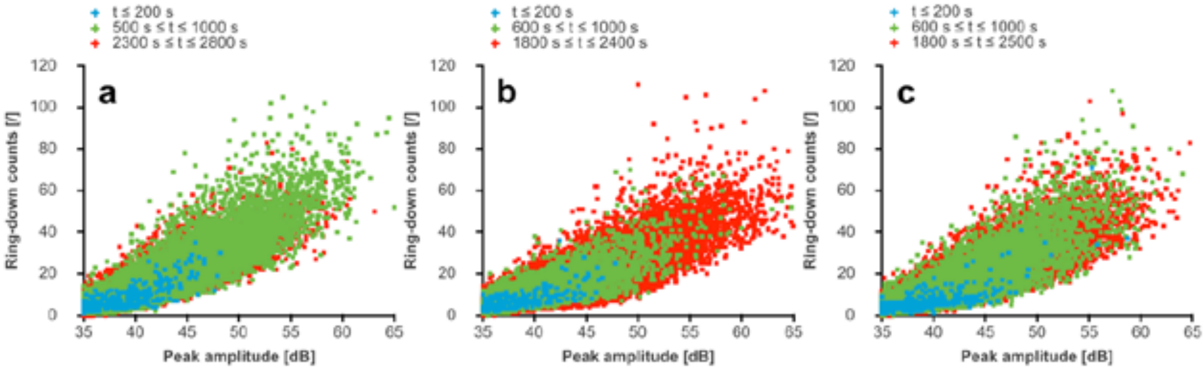

Fig. 6. Peak amplitude versus ring-down counts cross-plots of the AE during tensile deformation of commercially pure titanium at room temperature parallel to the (a) RD (b) TD and (c) 45D. The colors correspond to different time intervals during the deformation and are linked to mechanical deformation events. The blue points correspond to the onset of plastic deformation. The green points correspond to the time interval during which the UTS is reached. The red points correspond to the appearance of macroscopic necking.

In particular, 88.7% of these signals that have a peak amplitude larger than 50 dB are ‘red’ signals, meaning they originate during macroscopic necking. The ’red’ signals also make up 92.3% of all signals with a peak amplitude larger than 55 dB. Signal localization revealed that the origin of nearly all ‘red’ signals is found in a zone that is about 2 cm long, which demonstrates that the ‘red’ signals are localized in the necking zone and can indeed be linked to the macroscopic necking of the tensile specimen. This necking has caused a specific AE response in TD as seen in the second peak of fig. 3b and the anomalous behavior of the minority signal parameters in fig. 5b. However, in the other directions no such different AE response, nor difference in signal parameters was observed. This anisotropy can be explained by a deformation mechanism that is only activated during the macroscopic necking in the TD, which does not yet occur during uniform plastic deformation. Based solely on the AE results, no such change in deformation mechanism would be expected in RD and 45D. This also implies that the activity of the deformation mechanisms and in particular their evolution with increasing strain in TD, must be orientation-dependent.

AE cannot reveal what these deformation mechanisms exactly are. In order to couple these observations to the microstructural deformation mechanisms, a second set of tensile tests was carried out to different maximal strain levels. The microstructure at these strain levels is investigated with EBSD. These levels are marked with vertical arrows in fig. 3. For the TD specimens, these strains are chosen to be immediately before and after the expected peak maxima (fig. 3b) and just before the strain to failure. For the other specimens, the strain levels were chosen before and after the beginning and the end of the plateaus (fig. 3a and 3c) and one strain level in the middle of the plateau. Fig. 7 shows image quality maps of the deformed tensile specimens in RD, TD and 45D respectively. The twin boundaries are marked with colored lines.

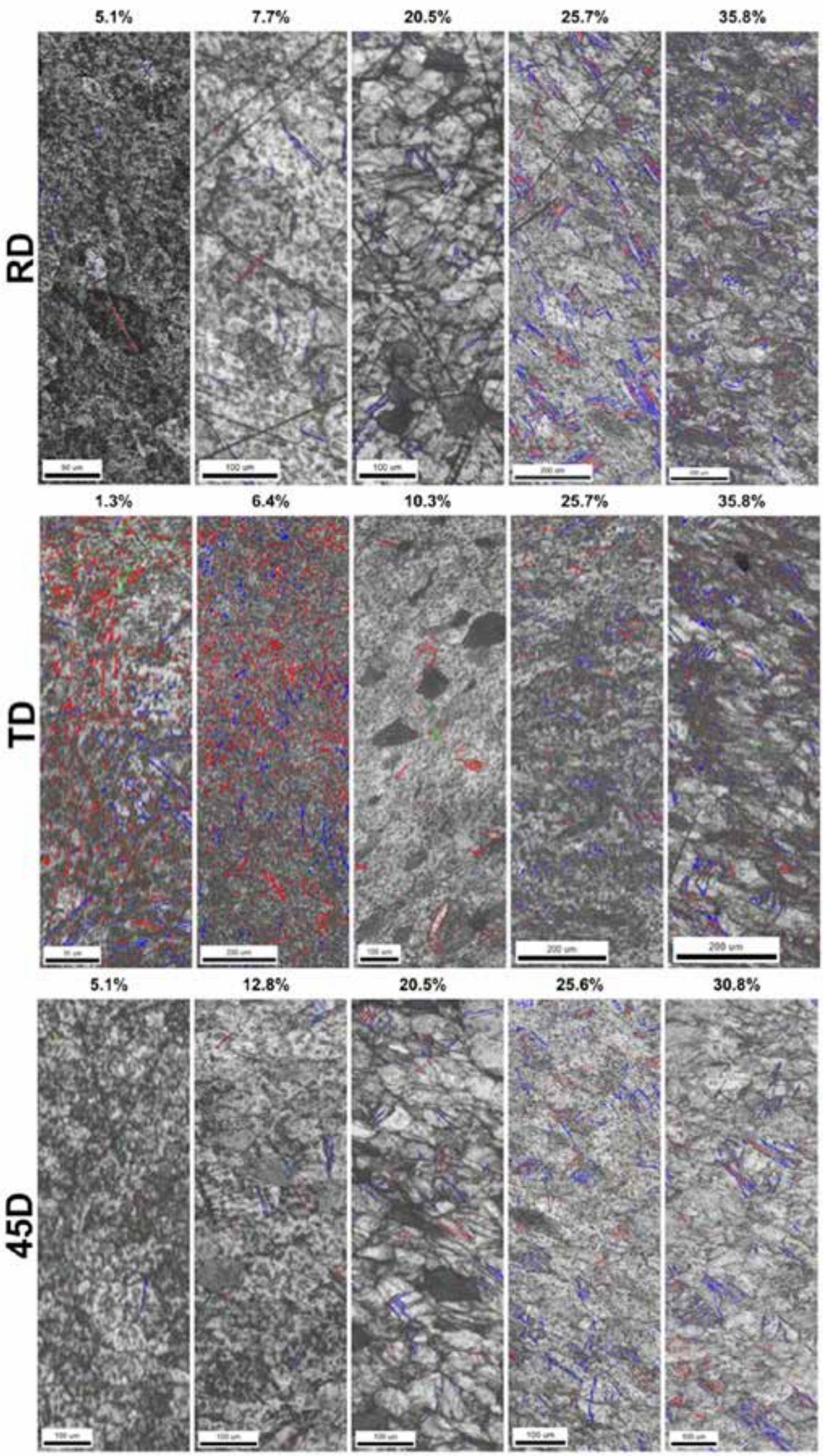
5.1%
7.7%
20.5%
25.7%
35.8%
RD
1.3%
6.4%
10.3%
25.7%
35.8%
TD
5.1%
12.8%
20.5%
25.6%
30.8%
45D

Fig. 7. EBSD image quality maps of tensile specimens deformed at room temperature until different strains with the load direction parallel to the rolling direction (RD), transversal direction (TD) and under an angle of 45° with the rolling direction in the rolling plane (45D). Twin grain boundaries are colored: tensile twins in red, compression twins in blue and compression twins in green. Deviations up to 5° from the theoretical K1 twinning planes and theoretical misorientations according to [3] are allowed.

4. Discussion

Partridge [3] reported that deformation twinning in titanium mainly occurs in the $\{10\bar{1}2\}$, $\{11\bar{2}1\}$ and $\{11\bar{2}2\}$ twinning planes. The magnitude of the twinning shear in these planes are 0.167, 0.638 and 0.225 respectively. These twins have already been observed in different studies [10-15]. Here, mainly $\{10\bar{1}2\}$ tensile twins with a misorientation of 90° and $\{11\bar{2}2\}$ compression twins with a misorientation of 65° are observed, in agreement with the theoretical values (94°52' and 63°58' respectively) [3]. Small deviations up to 5° from the theoretical twinning plane and theoretical misorientations are allowed. These deviations can be attributed to the relative rotation of the twins and other grains during further deformation. The twinning characteristics seem to be orientation-dependent. In RD and 45D twinning is dominated $\{11\bar{2}2\}$ by compression twins, while in TD twinning is dominated by $\{10\bar{1}2\}$ tensile twins. This observation is in accordance with other EBSD measurements [10,15,16] and crystal plasticity simulations [17].

The twinning activity appears to be low in RD and 45D until large strains (> 25%) are reached. Few twins are observed at a time in the microstructure. The twins are exclusively $\{11\bar{2}2\}$ twins in RD, but a combination of $\{11\bar{2}2\}$ twins and $\{10\bar{1}2\}$ twins appears in 45D, although $\{11\bar{2}2\}$ twins are the dominant type. Due to the generally low number of twins in RD and 45D the number of twins in consecutive scans and specimens shows a significant relative variability. Despite the large relative variations in the twin activity, the absolute number of twins remains low in general. This statement is backed by the AE data and fits the observation of the plateaus in fig. 3a and fig. 3c. The slightly larger width of $\{11\bar{2}2\}$ twins in RD, compared to 45D and the larger twinning shear of $\{11\bar{2}2\}$ twins compared to $\{10\bar{1}2\}$ twins [11] could explain the higher AE event rate and larger amplitudes in RD. For large strains (> 25%) the specimens showed macroscopic necking and the microstructure inside this necking zone was investigated. The microstructure inside the necking zone is composed of elongated grains which show a larger twinning activity. In both RD and 45D more $\{10\bar{1}2\}$ twins are present. However, in the AE no change in event rate or signal parameters is observed in the whole specimen, indicating that the increased $\{10\bar{1}2\}$ twinning is only happening locally in the necking zone.

The twinning evolution in TD is significantly different. Even at small deformations (1.3% strain) extensive twinning is observed. Besides $\{11\bar{2}2\}$ compression twins, a large fraction of $\{10\bar{1}2\}$ tensile twins is present. A small fraction of $\{11\bar{2}1\}$ compression twins is also distinguished. The twins are smaller in size than the twins in RD and 45D. Because the $\{10\bar{1}2\}$ twins result in less shear, their contribution to the deformation and, therefore, their associated deformation energy is smaller than $\{11\bar{2}2\}$ twins. The resulting AE signals in TD have a reduced energy and therefore lower amplitude for the same signal duration as compared to the signals in RD and 45D (fig. 5). It is likely that a larger fraction of those signals cannot exceed the threshold set for the amplitude and are blocked by the noise filter, resulting in a reduced AE event rate, as seen in fig. 3b. The twinning activity has decreased significantly at an intermediate strain of 10.3%, which coincides with the first AE peak in fig.

3b. A transormation has occurred during which the many narrow $\{10\bar{1}2\}$ twins have been replaced by a relative low amount of wider $\{10\bar{1}2\}$ twins. It is unclear whether the disappearance of certain twins and growth of other twins is coupled (e.g. twin merging) or not. Detwinning phenomena have been observed in pure titanium under reversed loading conditions during which $\{10\bar{1}2\}$ twins were replaced by $\{11\bar{2}2\}$ twins and vice versa [14,15]. The nucleation of twins requires more shear stress than the subsequent growth [18] and the resulting AE signal amplitude will be larger for twin nucleation than twin growth [19]. An in-situ study of detwinning in an AZ31 magnesium alloy showed that the initiation of detwinning results in higher AE amplitudes when compared to twin shrinkage [20]. However, no reversed loading has been applied during the tensile tests, which renders this option highly unlikely. The exact mechanism behind the change in twinning conditions remains unknown. At large strains (>20%) when macroscopic necking occurs, the microstructure inside the necking zone is dominated by $\{11\bar{2}2\}$ compression twins and the AE behavior becomes similar to the behavior observed in RD and 45D, as shown in fig. 6. The change in twinning mode also appears to be strongly localized inside the necking zone. It is suggested that the initial texture in the TD is unfavorable to the nucleation and growth of $\{11\bar{2}2\}$ twins. The $\{11\bar{2}2\}$ twins dominate the microstructure in RD and 45D suggesting that the unfavorable textural effect is only present when the loading direction is close to the TD. If the angle between the loading direction and the TD is increased, the unfavorable textural effect seems to disappear fast. When this angle reaches 45°, which is the case for the 45D specimens, the textural effect has already disappeared. The appearance of a majority fraction $\{11\bar{2}2\}$ twins in the TD in the necking zone can be attributed to the complex triaxial stress state present in the necking zone. The inhomogeneous deformation causes the local stress state to deviate significantly from the homogeneous uniaxial stress state. Therefore, the unfavorably oriented grains, which initially have low Schmid factors in the uniaxial stress state, can locally have higher Schmid factors in the triaxial stress state and can accommodate $\{11\bar{2}2\}$ twinning. Outside the necking zone the uniaxial stress state and consequently low Schmid factors are preserved. Therefore $\{11\bar{2}2\}$ twinning is not observed at all.

The low activity of $\{11\bar{2}2\}$ twins in RD and 45D corresponds to increased strain hardening and a large failure strain values, whereas the high activity of $\{10\bar{1}2\}$ twins in the TD corresponds to decreased strain hardening and smaller failure strain values in agreement to other experimental work. However, besides the twinning modes, the influence of the anisotropy on the dislocation motion and slip systems [3,8,17] must also be taken into account to correctly explain the full stress-strain behavior. The crystal-plasticity finite element simulation of Hama et al. [17] assumes a strong basal texture in which the c-axes of the grains are tilted between 20° and 40° from the plate normal direction to the TD and simulates the relative activity of various dislocation gliding mechanisms, $\{10\bar{1}2\}$ twinning and $\{11\bar{2}2\}$ twinning in RD and TD until a true strain of 9% is reached. In RD the relative activity of $\{10\bar{1}2\}$ twinning is nearly zero during the entire deformation, while the relative activity of $\{11\bar{2}2\}$ increases to 0.15 at 2% true strain and remains nearly constant during the subsequent deformation. In TD the relative activity of $\{10\bar{1}2\}$ increases fast to 0.20 at under 1% true strain, but is seen to decrease with increasing strain. At 6% true strain the relative activity has dropped under 0.10. The relative activity of $\{11\bar{2}2\}$ is small but non-zero and is seen to continuously increase, albeit slowly. These simulation results are in agreement with our data in the simulated strain range, highlighting the dependence of twinning on the texture.

5. Conclusion

The deformation mechanisms of commercially pure titanium subjected to uniaxial tensile load were investigated by combining in-situ AE measurements with EBSD investigations. The following conclusions could be drawn:

(i) A simple plateau-shaped AE response is observed when the tensile load is applied in RD and 45D. The signal characteristics and intensity remain relatively constant during the deformation. The deformation microstructure is dominated by $\{11\bar{2}2\}$ compression twins.

(ii) Different AE response and twinning mechanisms were observed when the tensile load is applied in the TD, compared to RD and 45D. Both the AE event rate and signal parameters follow a continuous upward trend exhibiting two distinct maxima. The first peak is associated with the transformation of many thin $\{10\bar{1}2\}$ tensile twins into a few broad $\{10\bar{1}2\}$ twins, while the second peak is associated with the appearance of $\{11\bar{2}2\}$ twins in the necking zone.

(iii) The difference in twinning mechanisms and the resulting AE responses are closely related to the texture and stress state. $\{11\bar{2}2\}$ twinning is unfavorable in the TD as the texture is unfavorably aligned towards the uniaxial stress state and $\{10\bar{1}2\}$ twinning is initiated. Once the loading direction is rotated away from the TD, the $\{11\bar{2}2\}$ twinning becomes increasingly dominant. The comparable AE and twinning behavior in the RD and 45D suggest that a small angle between the load direction and the TD is already sufficient to allow $\{11\bar{2}2\}$ twinning. Additionally, during macroscopic necking, the stress state inside the necking zone becomes complex and triaxial and the disadvantageous texture alignment disappears. Extensive $\{11\bar{2}2\}$ twinning is then observed as well in the necking zone, regardless of the (in-plane) loading direction.

References:

[1] von Mises R., Mechanik der plastischen Formänderung von Kristallen, Z. Angew. Math. Me., Vol. 8, 1928, 161-185

[2] Yoo M.H., Slip, twinning, and fracture in hexagonal close-packed metals, Metall. Trans. A, Vol. 12, 1981, 409-418

[3] Partridge P.G., The crystallography and deformation modes of hexagonal close-packed metals, Int. Mater. Rev., Vol. 118, 1967, 169-194

[4] Wevers M., Listening to the sound of materials: Acoustic emission for the analysis of material behaviour, NDT & E Int., Vol. 30, 1997, 99-106

[5] Máthis K., Chmelík F., Janeček M., Hadzima B., Trojanová Z., Lukáč P., Investigating deformation processes in AM60 magnesium alloy using the acoustic emission technique, Acta Mater., Vol. 54, 2006, 5361-5366

[6] Meza-García E., Dobroň P., Bohlen J., Letzig D., Chmelík F., Lukáč P., Kainer K.U., Deformation mechanisms in an AZ31 cast magnesium alloy as investigated by the acoustic

emission technique, Mat. Sci. Eng. A-Struct., Vol. 462, 2007 297-301

[7] Roth A., Lebyodkin M.A., Lebedkina T.A., Lecomte J.S., Richeton T., Amouzou K.E.K., Mechanisms of anisotropy of mechanical properties of α-titanium in tension conditions, Mat. Sci. Eng. A-Struct., Vol. 596, 2014, 236-243

[8] Nixon M.E., Cazacu O., Lebensohn R.A., Anisotropic response of high-purity α-titanium: Experimental characterization and constitutive modeling, Int. J. Plasticity, Vol. 26, 2010, 516-532

[9] Murasawa G., Morimoto T., Yoneyama S., Nucleation and Growth Behavior of Twin Region Around Yield Point of Polycrystalline Pure Ti, Exp. Mech., Vol. 52, 2012, 503-512

[10] Wronski S., Jedrychowski M., Tarasiuk J., Bacroix B., Microstructure evolution of titanium after tensile and recrystallisation, Mat. Sci. Eng. A-Struct., Vol. 692, 2017, 113-126

[11] Nemat-Nasser S., Guo W.G., Cheng J.Y., Mechanical properties and deformation mechanisms of a commercially pure titanium, Acta Mater., Vol. 47, 1999, 3705-3720

[12] Salem A.A., Kalidindi S.R., Doherty R.D., Strain hardening of titanium: role of deformation twinning, Acta Mater., Vol. 51, 2003, 4225-4237

[13] Tirry W., Bouvier S., Benmhenni N., Hammami W., Habraken A.M., Coghe F., Schryvers D., Rabet L., Twinning in pure Ti subjected to monotonic simple shear deformation, Mater. Charact., Vol. 72, 2012, 24-36

[14] Chun Y.B., Yu S.H., Semiatin S.L., Hwang S.K., Effect of deformation twinning on microstructure and texture evolution during cold rolling of CP-titanium, Mat. Sci. Eng. A-Struct., Vol. 398, 2005, 209-219

[15] Hama T., Nagao H., Kobuki A., Fujimoto H., Takuda H., Work-hardening and twinning behaviors in a commercially pure titanium sheet under various loading paths, Mat. Sci. Eng. A-Struct., Vol. 620, 2015, 390–398

[16] Yi N., Hama T., Kobuki A., Fujimoto H., Takuda H., Anisotropic deformation behavior under various strain paths in commercially pure titanium Grade 1 and Grade 2 sheets, Mat. Sci. Eng. A-Struct., Vol. 655 ,2016, 70-85

[17] Hama T., Kobuki A., Takuda H., Crystal-plasticity finite-element analysis of anisotropic deformation behavior in a commercially pure titanium Grade 1 sheet, Int. J. Plasticity, Vol. 91, 2017, 77-108

[18] Pirouz P., Lawlor B.F., Geipel T., Bilde-Sørensen J.B., Heuer A.H., Lagerlo K.P.D., On Basal slip and basal twinning in sapphire (α-Al2O3)—II. A new model of basal twinning, Acta Mater., Vol. 44, 1996, 2153-2164

[19] Li Y., Enoki M., Evaluation of the Twinning Behavior of Polycrystalline Magnesium at Room Temperature by Acoustic Emission, Mater. Trans., Vol. 48, 2007, 1215-1220

[20] Yasutomi T., Enoki M., In-situ evaluation of detwinning behavior in extruded AZ31 Mg alloy by AE, Mater. Trans., Vol. 53, 2012, 1611-1616